Simulation of excited-state formation of hydrogen in transmission of relativistic H^- ions through thin foils

Benoit Gervais,[1,2] Carlos O. Reinhold,[2,3] and Joachim Burgdörfer[2,3]
[1]*Centre Interdisciplinaire de Recherches avec les Ions Lourds, Laboratoire Mixte CEA-CNRS, rue C. Bloch, Boîte Postale 5133, 14040 Caen Cedex, France*
[2]*Department of Physics, University of Tennessee, Knoxville, Tennessee 37996-1200*
[3]*Oak Ridge National Laboratory, Oak Ridge, Tennessee 37831-6377*
(Received 8 June 1995)

We present a theoretical description of the formation of excited states H(n) due to the interaction of relativistic H^- ions with thin foils. The classical transport theory based on a Monte Carlo solution of a Langevin equation is generalized to relativistic speeds of the projectile. Relativistic corrections are introduced to both collision dynamics and kinematics. The n distribution of excited states, H(n), is studied as a function of the foil thickness and compared with recent experimental data.

PACS number(s): 34.10.+x

I. INTRODUCTION

Conversion of moderately relativistic H^- beams with energies between 100 MeV and 1 GeV into H^+ for injection into proton storage rings (PSR) is accomplished by transmission through thin self-supporting foils. The thickness of these foils is typically limited to a few hundred $\mu g/cm^2$ ($1\ \mu g/cm^2 \simeq 50$ Å $\simeq 95$ a.u.) in order to minimize the degrading of the beam due to energy and angular straggling. This, in turn, limits the efficiency of the conversion. Typically 10% of the projectiles still exit as fast neutrals (H^0) a fraction of which is in an excited state H(n) [1]. A significant neutral component is of considerable concern for high-current injection as envisioned for spallation-neutron sources: Moderately excited hydrogen, H($n \geqslant 3$), can be easily field stripped in the first bending magnet of the PSR, possessing therefore an ill-defined magnetic rigidity and causing beam loss and high levels of radiation near the first turn due to collisions with the walls. The determination of the excited-state distribution H(n) is therefore of considerable importance. We present in the following the first microscopic simulation of the excited formation for relativistic H^- beams. Our calculation employs a relativistic generalization of a previously developed classical transport theory (CTT) [2]. This method employs a Monte Carlo solution of a microscopic Langevin equation describing multiple scattering inside the solid and can be viewed as a stochastic version of the classical-trajectory Monte Carlo (CTMC) method.

The extension to relativistic speeds discussed in this paper refers to both the collision dynamics and kinematics. One qualitatively new feature is the inclusion of transverse electromagnetic excitations of the dielectric medium. As we will show below, their contribution at moderately relativistic energy $\lesssim 1$ GeV corresponding to a relativistic γ factor of $\gamma \leqslant 2$ remains, however, small. We furthermore extend the classical transport simulation to the evolution of two-electron initial states of H^- by treating the detachment as a precursor to the excited-state evolution of H(n).

We will apply the theoretical description to recent experimental data [3] from the High-Resolution Atomic Beam Facility (HIRAB) at the Los Alamos Meson Factory (LAMPF) for H^- with energies between 200 and 800 MeV. We find reasonably good agreement between experiment and theory. Atomic units are used unless otherwise stated. A preliminary report on this work has been given in Ref. [4].

II. THEORY

The theoretical description of the excited-state formation employs a number of simplifying assumptions which render this seemingly complex problem numerically tractable.

(a) The conversion from H^- to H^+ proceeds in a two-step process of sequential collisions with the medium, i.e., with electrons and/or nuclei of the atoms in the foil.

$$H^- \rightarrow H(n) + e^-, \tag{1a}$$

$$H(n) \rightarrow H^+ + e^-. \tag{1b}$$

This assumption is well justified in view of the observation that double ionization of H^- by a single charged-particle collision or photon absorption in the gas phase accounts only for about 1% of all ionizing collisions [5]. This so-called ''shake-off'' probability has been theoretically and experimentally investigated for He, the closest isoelectronic partner. The shake-off probabilities range, depending on the ionizing agent, between 0.26% [6,7] for the charged particles and 1.66% [5,8,9] for photoionization at high energies. Since H^- possesses only one bound state, the detachment [Eq. (1a)] is assumed to be a one-step process occurring in a single collision. It may result not only in the ground state but in excited-state formation of hydrogen, H(n), due to ''shakeup'' of the second electron. The ionization of H(n) is, on the other hand, a result of a sequence of collisions with intermediate states $H(n) \rightarrow H(n') \cdots \rightarrow H^+$ [Eq. (1b)] because of the high density of states in a Coulomb field. The treatment of this collisional redistribution of excited states due to multiple scattering inside the foil is the primary goal of the relativistic transport theory. The initial detachment and shakeup provides initial conditions for the subsequent random walk in state space. The detachment [Eq. (1a)] and ionization process [Eq. (1b)] are treated as uncorrelated events. Specifically, the detached electron is assumed to be well

TABLE I. Mean free path for elastic λ_{el}, longitudinal inelastic λ_l, and transverse inelastic λ_{tr}, and total mean free path λ_0 of a quasifree electron as a function of velocity v and equivalent proton energy in a.u. Also given are the relativistic parameters $\beta=v/c$ and $\gamma=[1-(v/c)^2]^{-1/2}$.

E (MeV)	v	β	γ	λ_{el}	λ_l	λ_{tr}	λ_0
226	81.10	0.592	1.24	4315	2261	1.29×10^5	1467
500	103.85	0.758	1.53	7075	3523	0.71×10^5	2276
581	107.73	0.786	1.62	7614	3770	0.66×10^5	2428
716	112.75	0.823	1.76	8340	4102	0.60×10^5	2629
800	115.35	0.842	1.85	8729	4279	0.58×10^5	2743

separated from H(n) such that it has no influence on the subsequent collisional redistribution among hydrogenic states.

(b) We employ classical relativistic dynamics in the transport theory treating the multiple scattering sequence. Accordingly, the initial detachment process generates an initial phase-space distribution which is then propagated according to classical dynamics. The mapping onto initial and final quantum states is performed by appropriate binning of the phase space. The validity of a classical description of multiple scattering requires that the collisional momentum transfer Δp satisfies the uncertainty relation [10]

$$\Delta p\langle r\rangle_n \gg 1, \tag{2}$$

where $\langle r\rangle_n$ is the radius of the initial state. A useful and somewhat more stringent criterion follows from the requirement [10] that Δp is of the order of the orbital momentum p_n, i.e., $\Delta p/p_n \gtrsim 0.5$. As will be shown below, this condition is well satisfied for the collision systems under investigation for excited states H ($n>2$) but only marginally so for the ground state H ($n=1$). Possible quantum corrections would have to be treated within a quantum version of the CTT. Development of such a quantum transport theory for the transport is a formidable task and a simplified version restricted to low-lying bound states is currently being developed.

A. Collisional detachment and shakeup

The first step [Eq. (1a)], i.e., the collisional detachment of H^- $(1s,1s')$, proceeds predominantly by ejection of the loosely bound electron $(1s')$ in collisions with electrons or nuclei of the carbon foil. The nonequivalent configuration of the two-electron state $(1s,1s')$ of H^- plays a crucial role in the description of ''shakeup'' and of the initial phase-space distribution. Because of the small binding energy $\epsilon_{1s'}=0.0275$ a.u. relative to the neutral hydrogen core and the relativistic collision speed ($v_p=80$–115 a.u.), the detachment cross section σ_D, or equivalently the inverse mean free path λ_D^{-1} for collisional detachment of H^-, can be determined from the total inverse mean free path λ_0^{-1} of a quasifree electron in carbon,

$$\lambda_D^{-1}=N\sigma_D \cong \lambda_0^{-1}, \tag{3}$$

where N is the number density ($N\simeq 9.9\times10^{22}/\mathrm{cm}^3$). The inverse mean free path λ_0^{-1} consists of contributions due to quasielastic scattering at a screened nucleus of carbon atoms, λ_{el}^{-1}, and due to inelastic scattering at core electrons and valence electrons, λ_i^{-1}. The term (in)elastic process refers here to the energy transfer to the medium. Calculation of differential and integral inverse mean free paths (IMFP) in linear response theory, or equivalently, in Born approximation, in the relativistic regime will be discussed in Sec. III. Differential inverse mean free paths are sometimes referred to as collision kernels in the context of transport equations. They provide the basic scattering information for the detachment and the excitation and ionization by multiple scattering. The quasifree electron approximation (3) can be directly tested by comparing with the exponential decay rate of the H^- fraction as a function of the foil thickness x,

$$P_{H^-}(x)=e^{-x/\lambda_D}\simeq e^{-z/\lambda_0}, \tag{4}$$

with the one calculated from the mean free path for free electrons (see Table I). Experimental values for λ_D^{-1} at 800 MeV and theoretical values for λ_0^{-1} ($\cong 3.7\times10^{-4}$) are indistinguishable within the experimental resolution. We therefore simulate the detachment step by the transport of a quasifree electron through the solid whereby each elastic or inelastic collision event results in the destruction of H^-. An explicit treatment of the two-electron classical dynamics of H^- is thereby circumvented. Equation (4) gives directly the source function of neutrals $S(x)$ per unit path length,

$$S(x)=\frac{dP_H(x)}{dx}=-\frac{dP_{H^-}(x)}{dx}, \tag{5}$$

of initial conditions for the transport of hydrogenic electrons.

In addition to the total source strength, information on the relative distribution among hydrogenic states P_{nlm} is required. Starting point of the analysis of this ''shakeup'' distribution is the first Born approximation with a two-electron transition amplitude

$$t_{i\to(\vec{k}_f,nlm)}=\langle\psi(\vec{k}_f,nlm)|V|\psi_i\rangle, \tag{6}$$

where V denotes the sum over all interactions between the electrons in H^- with the screened target nuclei and with the core and valence electrons of the carbon atoms. Highly correlated initial wave functions, ψ_i for the H^- bound state as well as approximately correlated final states representing excitation and detachment should be employed. The resulting cross section must be integrated over all final momenta $\vec{k}_f$. In practice, such calculations are very tedious and have been rigorously performed only for double ionization of helium by a bare Coulomb interaction with a structureless projectile [7]. A simpler approximation is provided by the gen-

eralized shake approximation [11]. Accordingly, the probability for shakeup into a hydrogen state nlm during emission of a second electron with momentum $\vec{k}_f$ described by a plane wave is given by the projection

$$P^{(S)}_{nlm}(\vec{k}_f)=C(\vec{k}_f)|\langle \vec{k}_f,nlm|\psi_i\rangle|^2. \tag{7}$$

The normalization constant $C(\vec{k}_f)$ is determined by the differential $\sigma_I(\vec{k}_f)$ and integral single ionization cross sections (σ_I), as

$$\sum_{nlm} P^{(S)}_{nlm}(\vec{k}_f)=\sigma_I(\vec{k}_f)/\sigma_I \tag{8}$$

leading to

$$C(\vec{k}_f)=\frac{\sigma_I(\vec{k}_f)}{\sigma_I}\left[\int d^3r\left|\int d^3r'\,\psi_i(\vec{r},\vec{r}')e^{-i\vec{k}_f\vec{r}'}\right|^2\right]^{-1}, \tag{9}$$

where we have used the closure property for the complete sum over bound and continuum states (Σ_{nlm}). A further simplification can be reached by neglecting the wave-number (or energy) dependence of the normalization constant $C(\vec{k}_f)$. The inclusive shakeup probability irrespective of the momentum of the outgoing electrons is then given by

$$P^{(S)}_{nlm}=\int d^3r\left|\int d^3r'\,\psi_i(\vec{r},\vec{r}')\phi^*_{nlm}(\vec{r}')\right|^2. \tag{10}$$

This generalized shake approximation has been previously used for relating the shakeup process by charged-particle collisions with the corresponding process by photon scattering beyond the dipole approximation [12]. This additional approximation tends to overemphasize the shakeup contribution resulting from fast electron emission. However, since the generalized shake approximation neglects correlations between the two electrons in the final state which are most important for slow electrons, it is not obvious how much of an improvement Eq. (7) compared to Eq. (10) would represent. We have therefore employed in our simulation the approximation (10) with the initial wave function ψ_i of Chandrasekhar [13]. This three-parameter wave function with the asymmetric exponents for nonequivalent electrons gives the binding energy (affinity) to within 6% of the exact value. The final wave functions are hydrogenic. We limit our calculation to the first excited states up to $n=3$. Higher excited states as well as double ionization are neglected since their shake probabilities are very small. The sudden approximation underlying the shake description of detachment [Eqs. (7) and (10)] is in line with the description of multiple collisions in terms of impulse momentum transfers employed in the CTT [see Eq. (14) below].

The source strength per unit path length for a given excited state nlm follows from Eqs. (5) and (10) as

$$S_{nlm}(x)=-\frac{dP_{\mathrm{H}^-}(x)}{dx}P^{(S)}_{nlm}. \tag{11}$$

This source strength can now be mapped onto a source strength of classical initial conditions, i.e., of phase-space density per unit length,

$$S^{\mathrm{cl}}_{nl}(\vec{r},\vec{p};x)=A\,\delta(E_n-H(\vec{r},\vec{p}))\,\theta(L-l)\,\theta(l+1-L), \tag{12}$$

where $H(\vec{r},\vec{p})$ is the hydrogenic Hamiltonian

$$H(\vec{r},\vec{p})=\frac{p^2}{2}-\frac{1}{r},$$

$\vec{L}=\vec{r}\times\vec{p}$ is the orbital angular momentum, θ is the unit step function, and A is the proper normalization constant such that the integration of Eq. (12) over phase-space variables $(\vec{r},\vec{p})$ yields Eq. (11). Since in the sudden shakeup process the initial position coordinate is confined to the radius of the $1s$ orbital, we have also tested the effect of the radial confinement of the initial phase-space distribution to radii less than $r_0\simeq 1.5$ a.u. by multiplying the right-hand side of Eq. (12) by a step function $\theta(r_0-r)$. We find the simulations to be quite insensitive to this modification of the initial conditions within ($\simeq$5%) and have therefore omitted this correction.

B. Excitation and ionization by multiple scattering

Collisional detachment and the resulting shakeup provide the initial conditions for the classical electron in hydrogen which is subject to multiple collisions in the solid. As a result the distribution of bound states created by the shake process is modified and ultimately ionized. We describe the evolution of the hydrogenic electron by a stochastic version of Newton's equation of motion, i.e., a microscopic Langevin equation [2],

$$\dot{\vec{v}}=-\frac{\vec{r}}{r^3}+\vec{F}_c(t), \tag{13}$$

where the first term describes the unscreened interaction with the electron with the proton and $\vec{F}_c(t)$ is a stochastic force which describes multiple scattering in the solid. Here and in the following $(\vec{r},\vec{v})$ denote the position and velocity vector of the electron in the projectile frame. At relativistic speeds $(v_p\lesssim c)$ relative to the laboratory frame, dynamical screening in the medium (the solid) is strongly suppressed and the bare electron-projectile nucleus Coulomb interaction can be used. We generate an ensemble of initial conditions with strength per unit length (number of phase points) according to Eq. (11). Their distribution in phase space is given by Eq. (12). Each phase-space point is propagated in time t according to Eq. (13). The physical description of the classical transport theory can be visualized as a "random flight" problem along a sequence of Kepler orbits [Fig. 1(a)] or equivalently as a random walk through bound and continuum states of the Coulomb problem [Fig. 1(b)]. During evolution in time t, the hydrogen atom travels a distance $x=v_p t\gamma_p$ through the solid where $\gamma_p=[1-(v_p/c)^2]^{-1/2}$. The point to be noted is that the collision dynamics in the projectile frame is entirely nonrelativistic since $v\ll c$. Relativistic effects enter through the stochastic force $\vec{F}_c(t)$ since the velocity of the electron in the laboratory frame is close to c, $v'\simeq v_p\lesssim c$ and therefore scattering of the projectile electron with the medium is governed by relativistic dynamics.

We describe the stochastic force in terms of a sequence of impulsive momentum transfers ("kicks")

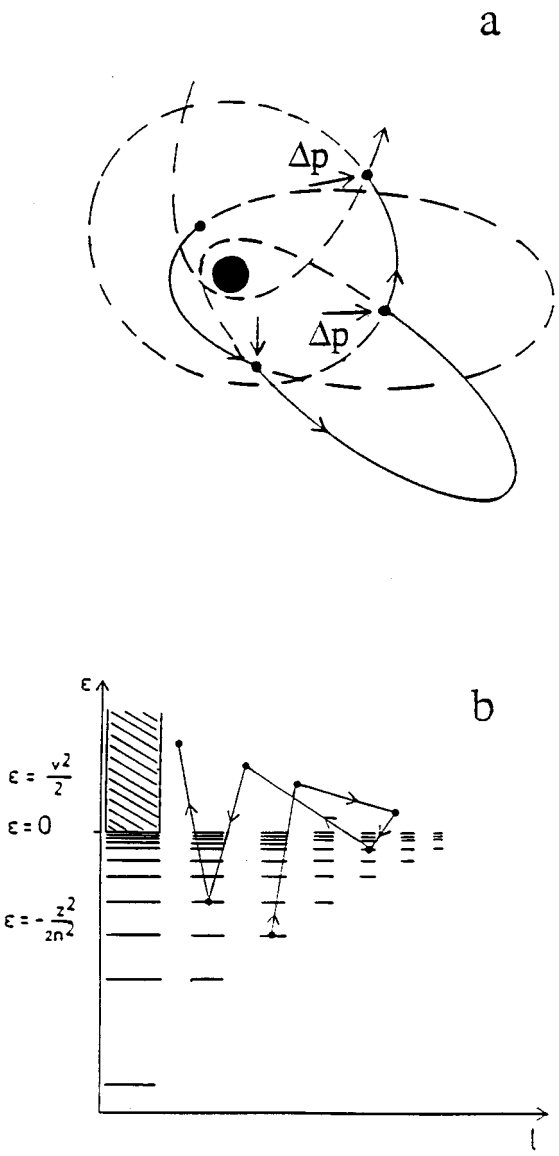

FIG. 1. Random walk of an electron in the hydrogen atom due to multiple scattering. (a) Sequence of classical Kepler orbits generated by collisional momentum transfers (''slingshot effect''), (b) random walk in the Coulomb state space (ϵ-l plane).

$$\vec{F}_c(t)=\sum_{\alpha}\sum_{i}\Delta\vec{p}_i^{\,\alpha}\delta(t-t_i^{\alpha}), \tag{14}$$

where $\Delta\vec{p}_i^{\,\alpha}$ is the stochastic momentum transfer per collision at the time t_t^{α}. The determination of $\vec{F}_c(t)$ is thereby reduced to that of a stochastic sequence of pairs $(\Delta\vec{p}_i^{\,\alpha},t_i^{\alpha})$. The approximation of the collisional interactions of fast electrons with target atoms in terms of instantaneous momentum transfers is based on the observation that the interaction is short ranged with the range determined by the static screening length in the medium (typically of the order of 1 a.u.). The corresponding collision time $t_c\simeq 1/v_p$ is short compared to the orbital period $t_n=2\pi\omega_n^{-1}=2\pi n^3$.

In Eq. (14) we have decomposed the sequence of collisional momentum transfers into three independent subsequences. One sequence ($\alpha=1$) refers to elastic electron-target core scattering while the others ($\alpha=2,3$) refer to inelastic electron-electron scattering resulting in longitudinal and transverse excitations of the medium. The sequence of collisional momentum transfers and collision times in the target frame $(\Delta p_i'^{\,\alpha},t_i'^{\,\alpha})$ is determined by relativistic collision dynamics. Lorentz transformation into the rest frame of the proton provides the input to Eq. (14). Details for the calculation of the $\Delta p_i'$ and t_i' will be given below. We neglect electron capture from the target. Capture cross sections are extremely small ($\leqslant 10^{-14}$ a.u.) in the range of velocities considered here. This applies to both mechanical capture (Thomas scattering [14]) and radiative capture [15]. The mapping of the evolved classical phase-space distribution back onto final quantum states proceeds via binning techniques well known from the CTMC method. If the classical action $n_c=(2|E|)^{-1/2}$ lies in the interval [16]

$$[n(n-\tfrac{1}{2})(n-1)]^{1/3}\leqslant n_c\leqslant[n(n+\tfrac{1}{2})(n+1)]^{1/3} \tag{15}$$

the event is ascribed the final quantum number n. For continuum states, which are included in the simulation, the kinetic energy at asympotically large distances should be binned.

III. INVERSE MEAN FREE PATH

The essential input for the simulation of the detachment process [Eq. (4)] as well as of the excited-state evolution described by the Langevin equation [Eqs. (13) and (14)] are the relativistic differential (DIMFP) and integral inverse mean free paths for quasi-free electrons. They determine the attenuation length of the initial H^- component, the probability distribution of collisional momentum transfers $\Delta\overrightarrow{p_i'^{\alpha}}$, and the time intervals (flight times) $\Delta t_i'^{\,\alpha}=t_{i+1}'^{\,\alpha}-t_i'^{\,\alpha}$, between these ''kicks.'' The DIMFP's are calculated in the frame of the medium and have to be Lorentz transformed to the projectile frame for use as input in Eq. (13). For notational simplicity we will omit all primes in this section with the understanding that all quantities refer to the laboratory frame. The DIMFP's to be used in the classical simulation will be calculated in first-order quantum perturbation theory, i.e., in Born approximation. In other words, the evolution of the atomic electron is calculated classically while the driving force for the random walk is determined by the quantum mechanics of electron-solid interactions.

We consider the following scattering processes.

(a) Elastic scattering ($\alpha=1$). Elastic scattering refers in the present context to zero energy transfer to target electrons. For elastic scattering ($\alpha=1$) we calculate $\lambda_{\rm el}^{-1}$ from scattering at an exponentially screened Coulomb potential, $V(r)=-Z_T\exp(-r/a)/r$, with a Thomas-Fermi screening radius $a=0.886Z_T^{-1/3}$ and Z_T the charge of the target nucleus ($Z_T=6$ for carbon). In the first-order Born approximation we have [2]

$$\frac{d\lambda_{\rm el}^{-1}}{dq}=\frac{8\pi Z_T^2N}{v^2}\frac{q}{[q^2+(1/a)^2]^2}. \tag{16}$$

The nonrelativistic expression in terms of the (relativistic) momentum transfer q agrees with the relativistic counterpart to a good degree of approximation [17]. Nontrivial relativis-

tic corrections become important only for ''hard'' collisions at small impact parameters which contribute little to the total cross section. They are, furthermore, of no relevance to the transport problem since hard collisions remove a phase-space point immediately from the relevant region in phase space near the projectile. According to Eq. (16), the integral IMFP scales as v^{-2},

$$\lambda_{\rm el}^{-1}=4\pi Z_T^2 N a^2/v^2. \tag{17}$$

(b) Longitudinal excitation ($\alpha=2$). Inelastic collisions of the projectile electron with the medium lead to electronic excitations in the medium, and hence, to modifications of the electromagnetic field due to the polarization of the medium. The dielectric response can be decomposed into a field component parallel and perpendicular to the wave vector $\vec{k}$ of the electromagnetic field. The parallel (or longitudinal) component E_l describes the electrostatic (irrotational, $\vec{\nabla}\times\vec{E}_l=0$) response while the transverse component $E_{\rm tr}$ (divergence-free, $\vec{\nabla}\vec{E}_{\rm tr}=0$) describes the electrodynamic response. At nonrelativistic velocities the electrostatic response completely dominates the energy transfer to the medium while at relativistic speeds the transverse electromagnetic excitations become increasingly important. The DIMFP as a function of energy transfer ω and momentum transfer q for electron scattering associated with longitudinal excitations is given in terms of the inverse dielectric function as [18,19]

$$\frac{d^2\lambda_l^{-1}}{d\omega\, dq}=\frac{2}{\pi v^2 q}\,{\rm Im}\left(-\frac{1}{\epsilon(q,\omega)}\right). \tag{18}$$

For the dielectric function we use a modified form of the approximation in terms of Drude functions due to Ashley *et al.* [20],

$$\epsilon^{-1}(q,\omega)=1-\sum_{i=1}^{5}\chi_i(q,\omega), \tag{19}$$

where each partial polarizability χ_i is given by the plasmon-pole approximation which includes dispersion,

$$\chi_i=\frac{\omega_{pi}^2}{[\omega_{oi}+c^2(\sqrt{q^2/c^2+1}-1)]^2-\omega^2-i\,\eta_i\omega}. \tag{20}$$

We use here the relativistic rather than the nonrelativistic $\omega(q)$ relation which describes the plasmon-pole position in the (q,ω) plane in the limit of large q. The parameters for the first four plasmon-pole terms $(\omega_{pi},\omega_{oi},\eta_i)$ are taken from Ref. [20]. A further term is added to account for the carbon K-shell excitation with the relevant parameters deduced from optical absorption data [21–23]. The real and the imaginary parts of the dielectric function are shown in Fig. 2 as a function of ω for different values of q. This approximation reproduces the main collective resonances and shell excitations observed in the optical energy loss spectrum. However, it does not properly represent low-frequency interband and intraband excitations [24]. The approximations [Eqs. (19) and (20)] satisfy the Thomas-Reiche-Kuhn sum rule. The integrated IMFP for longitudinal excitation scales as

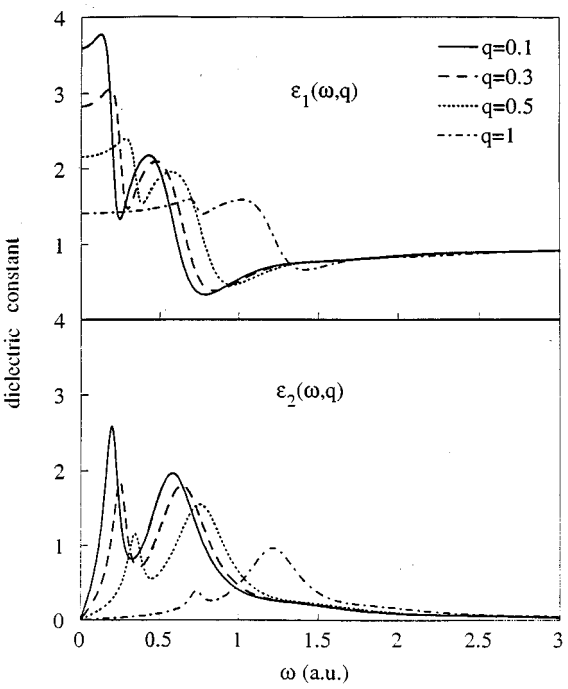

FIG. 2. Real and imaginary parts of the dielectric function of carbon versus the energy transfer ω, $\epsilon_1(\omega,q)$, and $\epsilon_2(\omega,q)$ for different momentum transfers $q=0.1$, 0.3, 0.5, and 1.

$$\lambda_l^{-1}=\frac{4\pi N Z_T}{v^2}\ln\frac{2v^2}{\langle\omega_0\rangle}, \tag{21}$$

where $\langle\omega_0\rangle$ denotes the average excitation energy.

(c) Transverse excitation ($\alpha=3$). The DIMFP for transverse excitation is given in terms of the complex dielectric function $\epsilon(q,\omega)=\epsilon_1(q,\omega)+i\,\epsilon_2(q,\omega)$ by [18,19]

$$\frac{d^2\lambda_{\rm tr}^{-1}}{d\omega\, dq}=\frac{2\beta^2 N}{\pi c^2 q}\,\frac{(1-\cos^2\delta)\epsilon_2\cos^2\delta}{(1-\beta^2\epsilon_1\cos^2\delta)^2+\beta^4\epsilon_2^2\cos^4\delta}, \tag{22}$$

where δ is the angle between $\vec{p}_1$ and $\vec{q}$,

$$\cos\delta=\frac{(p_1^2-p_2^2)+q^2}{2p_1 q}, \tag{23}$$

$\vec{p}_1$ and $\vec{p}_2$ are the momenta of the incident electron before and after the collision, $\vec{q}=\vec{p}_1-\vec{p}_2$, $\beta=v/c$, and $\vec{p}_1=\gamma\vec{v}$.

One prominent feature in the transverse excitation spectrum is the Čerenkov singularity. For small energy and momentum transfers, ϵ_2 is small and $d^2\lambda_{\rm tr}^{-1}/d\omega\, dq$ peaks near

$$1-\beta^2\epsilon_1\cos^2\delta\simeq 0, \tag{24}$$

which gives the dispersion relation for Čerenkov radiation. For energy transfers ω which are very small compared to c^2, Eq. (24) reduces to

$$\epsilon_1(\omega,q)^{1/2}=[\beta\,\cos\delta]^{-1}\approx\frac{2\gamma c q}{(2\omega\gamma+q^2)}. \tag{25}$$

In the ''optical'' limit of small momentum transfers $q^2\ll\omega$ the dispersion relation reads

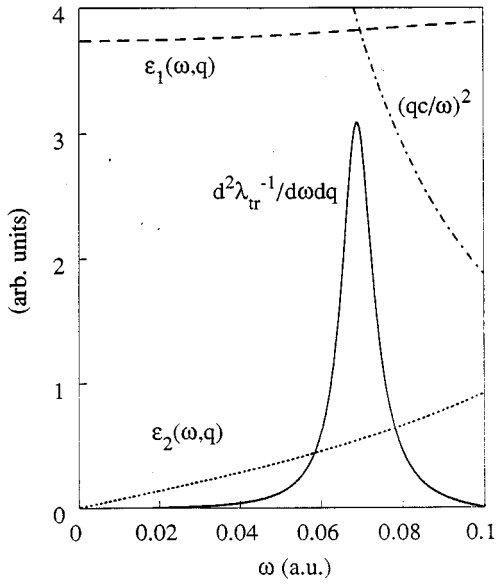

FIG. 3. Čerenkov peak in $d^2\lambda_{tr}^{-1}/d\omega\, dq$ versus the energy transfer ω for $q=10^{-3}$. Also shown are $\epsilon_1(\omega,q)$, $\epsilon_2(\omega,q)$, and the dispersion relation (26) for the Čerenkov effect at $v=100$ a.u.

$$\epsilon_1(\omega,q)^{1/2} \approx \frac{cq}{\omega}. \tag{26}$$

Since ϵ_1 is of the order of 1, the Čerenkov peak appears at very small momentum transfers q. On the other hand, the minimum momentum transfer in a collision, $q_{\min}$, may be well approximated by $q_{\min} \approx \omega/v$ at large velocities. Therefore the relevant region in the (q,ω) dispersion plane is delineated by

$$\epsilon_1(\omega,q)^{1/2} \approx \frac{cq}{\omega} \gtrsim \beta^{-1}. \tag{27}$$

The size of this region is limited further by the fact that with increasing $q, \epsilon_1(\omega,q)^{1/2}$ decreases (see Fig. 2). The behavior of $d^2\lambda_{tr}^{-1}/d\omega\, dq$ in the region of the Čerenkov singularity is illustrated in Fig. 3. The IMFP for transverse excitation scales in the region $\gamma \lesssim 2$ as v^2 (see Table I) and eventually dominates over the longitudinal excitations (whose IMFP scales as $v^{-2}\ln v^2$) in the highly relativistic regime. At moderate values of $\gamma \leqslant 2$ the two contributions are of comparable order of magnitude, i.e., this regime is close to the stopping power minimum.

The scaling behavior of λ_{tr}^{-1} is illustrated in terms of the ratio of the DIMFP for several velocities relative to the DIMFP at $v=103.85$ (Fig. 4). For the lowest velocity ($v=80$, $E_p=226$ MeV) we note, however, a drastic change of shape of the DIMFP, in particular at low-energy transfers. The latter is due to the disappearance of the Čerenkov singularity [see Eq. (27)]. A comparison of $d\lambda^{-1}/d\omega$, integrated over q, for longitudinal and transverse excitations (Fig. 5) indicates that transverse excitations contribute comparatively little to the energy loss of a fast electron at $v=100$ a.u. The mean values of the energy transfer are $\langle\omega\rangle_{tr}=0.8$ and $\langle\omega\rangle_l \simeq 2$. The comparison shows, furthermore, that at moderately relativistic values $\gamma \lesssim 2$, the contribution of transverse excitation is still relatively small compared to the longitudinal excitation.

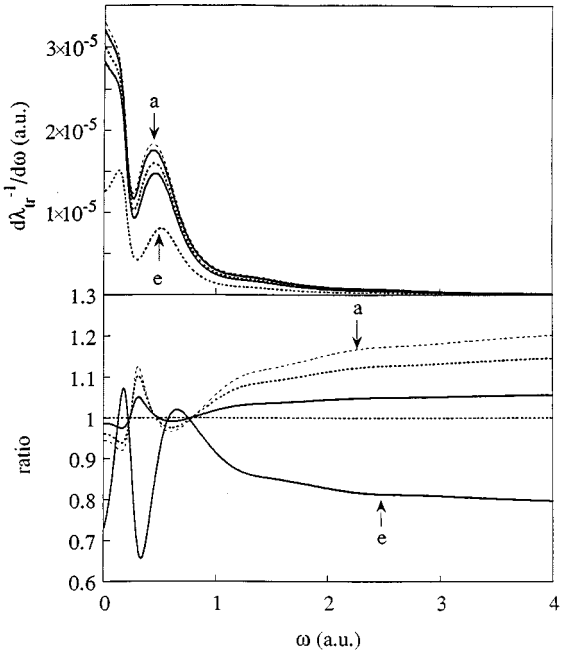

FIG. 4. $d\lambda_{tr}^{-1}/d\omega$ for different projectile velocities corresponding to proton energies of (a) $E_p=800$ MeV, (b) $E_p=716$ MeV, (c) $E_p=581$ MeV, (d) $E_p=500$ MeV, (e) $E_p=226$ MeV. The lower part of the figure shows the ratio of the DIMFP at a given energy E relative to DIMFP at 500 MeV multiplied by the inverse squared ratio of the velocities $[v(500\text{ MeV})/v(E_p)]^2$.

The DIMFP serves as input for the distribution functions of the collisional momentum transfer $W_\alpha(\Delta\vec{p})$. In order to construct $(\Delta\vec{p}=-\vec{q})$, the energy transfer ω and momentum transfer $q=|\Delta\vec{p}|$ must satisfy the relativistic (on shell)

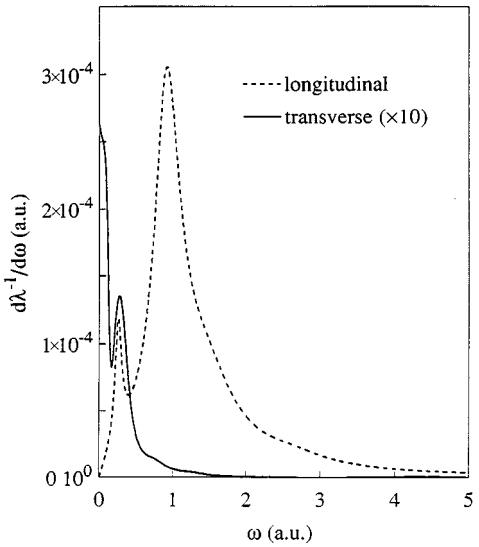

FIG. 5. DIMFP versus ω for the transverse and longitudinal inelastic excitations at $v=100$ a.u. The DIMFP for transverse excitations has been multiplied by 10 in order to facilitate comparison of the shapes of both curves.

energy-momentum dispersion relation for energies $E_{1,2}$ and momenta $\vec{p}_{1,2}$ before and after the collision,

$$\Delta E = E_1 - E_2 = \omega = (p_1^2 c^2 + c^4)^{1/2} - [(\vec{p}_1 - \vec{q})^2 c^2 + c^4]^{1/2}, \tag{28}$$

which yields

$$\Delta p_{\parallel} = \frac{\omega^2}{2c^2 \gamma v} - \frac{q^2}{2\gamma v} - \frac{\omega}{v} \tag{29}$$

and

$$\Delta p_{\perp}^2 = q^2 - \Delta p_{\parallel}^2. \tag{30}$$

The azimuthal angle of $\Delta \vec{p}_{\perp}$ is cyclic and therfore uniformly distributed. The probability distributions are proportional to the DIMFP,

$$W_{\alpha}(\Delta \vec{p}) \propto \frac{1}{q} \frac{d^2 \lambda_{\alpha}^{-1}}{d\omega \, dq}\bigg|_{q=\Delta p, \omega = \Delta E} \tag{31a}$$

for $\alpha = 2, 3$ and

$$W_{\mathrm{el}}(\Delta \vec{p}) \propto \frac{1}{q} \frac{d\lambda_{\mathrm{el}}^{-1}}{dq}\bigg|_{q=\Delta p} \tag{31b}$$

for $\alpha = 1$.

The elastic DIMFP [Eq. (31b)] depends only on Δp while the inelastic DIMFP [Eq. (31a)] depends on both ΔE and Δp. Accordingly, we construct one-or two-dimensional non-uniform random number distributions representing the DIMFP. The normalization is fixed through the relation between the IMFP and the time interval between collisions of the same type α,

$$(t_{i+1}^{\alpha} - t_i^{\alpha}) = \Delta t_{\alpha} = x'/v. \tag{32}$$

Assuming a homogeneous medium, the flight time Δt_{α}, or the distance x' traveled, between successive collisions follows a Poisson probability distribution

$$P_{\alpha}(x') = \lambda_{\alpha}^{-1} \exp(-x'/\lambda_{\alpha}). \tag{33}$$

Since inverse mean free paths are additive, the total inverse mean free path for quasifree electron scattering is

$$\lambda_0^{-1} = \sum_{\alpha=1}^{3} \lambda_{\alpha}^{-1}, \tag{34}$$

which determines the statistical distribution function for survival of the H^- fraction [Eqs. (3) and (4)].

IV. KINEMATICS

The collisional momentum transfers determined in the preceding section refer to the laboratory frame and will be denoted by primes, $\Delta \vec{p}'$, in the following. Their incorporation into the Langevin equation [Eq. (13)] of the CTT requires the Lorentz transformation of both the momentum transfer distribution and the flight time distributions.

From the definition of the mean free path in the laboratory frame,

$$\lambda' = \int_{t'(0)}^{t'} v' dt' = \int_0^{\Delta t} v' \frac{dt'}{dt} dt, \tag{35}$$

and the transformation between the target frame and projectile frame,

$$\frac{dt'}{dt} = \gamma_p \left(1 - \frac{\vec{v}_p \cdot \vec{v}}{c^2}\right), \tag{36}$$

the flight time becomes

$$\Delta t = \lambda' / \gamma_p v' \left(1 - \frac{\vec{v}_p \vec{v}}{c^2}\right). \tag{37}$$

Since the speed of the electron in the projectile frame is small ($v \ll c$) the path lengths of the electron and of the projectile are approximately equal and Eq. (37) reduces to

$$\Delta t = \lambda' / \gamma_p v_p = \Delta t' / \gamma_p. \tag{38}$$

Note that the flight time in the projectile frame is contracted because of the contraction of the mean free path, as seen in the projectile frame.

Expressed in terms of the velocity of the electron before ($\vec{v}_1' = \vec{v}'$) and after the collision ($\vec{v}_2'$) in the laboratory frame, the momentum transfer $\Delta \vec{p}'$, as determined by Eqs. (29) and (30) and now denoted by primed quantities, can be expressed as

$$\gamma_2' \vec{v}_2' = \gamma_1' \vec{v}_1' + \Delta \vec{p}', \tag{39}$$

where

$$\gamma_{1,2}' = \left(1 - \frac{v_{1,2}'^2}{c^2}\right)^{-1/2}. \tag{40}$$

The initial velocity in the target frame $\vec{v}_1'$ is given by the Lorentz transformation of $\vec{v}_1$,

$$v_{1\parallel}' = \frac{v_{1\parallel} + v_p}{1 + v_{1\parallel} v_p / c^2}, \tag{41}$$

$$v_{1\perp}' = \frac{v_{1\perp}}{\gamma_p (1 + v_{1\parallel} v_p / c^2)}, \tag{42}$$

The velocity after the collision in the laboratory frame is therefore

$$\vec{v}_2' = \frac{\gamma_1' \vec{v}_1' + \Delta \vec{p}'}{\sqrt{(\gamma_1' \vec{v}_1' + \Delta \vec{p}')^2 / c^2 + 1}}. \tag{43}$$

The velocity in the projectile frame follows from the inverse Lorentz transformation

$$v_{2\parallel} = \frac{v_{2\parallel}' - v_p}{1 - v_{2\parallel}' v_p / c^2} \tag{44}$$

and

$$v_{2\perp} = \frac{v_{2\perp}'}{\gamma_p (1 - v_{2\parallel}' v_p / c^2)}. \tag{45}$$

Finally, the collisional momentum transfer in the projectile frame is given for small velocities by

$$\Delta\vec{p}=\vec{v}_2-\vec{v}_1. \tag{46}$$

It is instructive to compare the resulting relativistic with the nonrelativistic collisional momentum transfer $\Delta\vec{p}$ [2]. To simplify the analysis we consider the case of an electron initially at rest in the projectile frame ($\vec{v}_1=0$). To the lowest order in $\Delta p'_\parallel/c$ and in $\Delta p'^2/2c$ we obtain the following expressions for the parallel and the perpendicular components of the velocity and momentum transfer:

$$\Delta p_\parallel=v_{2\parallel}=\frac{\Delta p'_\parallel}{\gamma_p}-\frac{v}{c}\frac{\Delta p'^2}{2c} \tag{47}$$

and

$$\Delta p_\perp=v_{2\perp}=\Delta p'_\perp. \tag{48}$$

Using the expression of $\Delta p'_\parallel$ in terms of the energy and momentum transfer [Eq. (29)], we find to first order in $\Delta p'/v_p$

$$v_{2\parallel}=-\frac{\Delta p'^2}{2v_p}-\frac{\omega'}{\gamma_p}. \tag{49}$$

This agrees with the nonrelativistic counterpart [see Ref. [2], Eq. (37)] up to a factor γ_p in the denominator in the second term of Eq. (49). This observation has the following implications.

(a) For elastic scattering ($\omega'=0$) the second term in Eq. (49) is absent. The relativistic and nonrelativistic transverse [Eq. (48)] and longitudinal [Eq. (49)] momentum transfers are identical.

(b) For inelastic scattering, the dominant region in the energy-momentum transfer plane lies near $q^2=\Delta p'^2\ll\omega'$. Therefore, the longitudinal momentum transfer is compressed by a factor $1/\gamma_p$ [Eq. (49)] while the transverse momentum transfer remains unchanged.

Figure 6 illustrates the compression effect of the frame transformation on the distribution $W(\Delta p_\parallel)$ of the parallel component of the momentum transfer for elastic and inelastic collisions. While the longitudinal momentum transfer for elastic collisions is unchanged, it is compressed by approximately the factor $1/\gamma_p$ for inelastic collisions. In both cases of elastic and inelastic scattering the perpendicular momentum transfer is only marginally changed. Since, furthermore, the perpendicular component is larger than the parallel component of the momentum transfer, the total momentum transfer remains almost unaffected by the frame transformation.

The invariance of the transverse momentum $\Delta p_\perp$ under frame transformation [Eq. (48)] should not be confused with the compression of scattering angle θ' due to relativistic kinematics. The relation between the angle θ', the momentum transfer, and the velocity may be derived from the conservation of momentum for the collision in the laboratory frame. In the case of elastic collisions we have

$$\sin\left(\frac{\theta'}{2}\right)=\frac{\Delta p'}{2\gamma v'}. \tag{50}$$

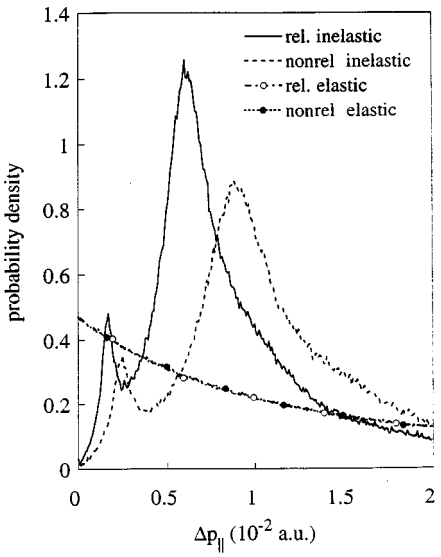

FIG. 6. Influence of the frame transformation on the distribution function $W(\Delta p_\parallel)$ for the parallel component of the momentum transfer $\Delta p_\parallel$ for inelastic longitudinal and elastic collisions at $v=100$ a.u. Shown are $W_\alpha(\Delta p_\parallel)$ with relativistic and nonrelativistic frame transformations for elastic collisions and inelastic longitudinal excitations.

The angle of deflection of the electron, θ', is reduced by a factor γ, compared to the nonrelativistic angle of deflection. This effect is due to the effective mass increase of the electron at relativistic velocities.

Characteristic differences in the distribution functions, $W_\alpha(|\Delta p|)$, for elastic, longitudinal, and transverse inelastic momentum transfers are displayed in Fig. 7. For inelastic transfers, the distribution functions W_α [Eq. (31a)] are integrated over all ΔE. The transverse excitation peaks at small momentum transfers $|\Delta p|\ll 1$ while the largest momentum transfers result from elastic scattering. At $v=100$ a.u. the mean values are $\langle\Delta p\rangle_{\rm tr}=1.11\times10^{-2}$, $\langle\Delta p\rangle_l\approx1.6$, and $\langle\Delta p\rangle_{\rm el}=3.2$. These differences play a significant role in as-

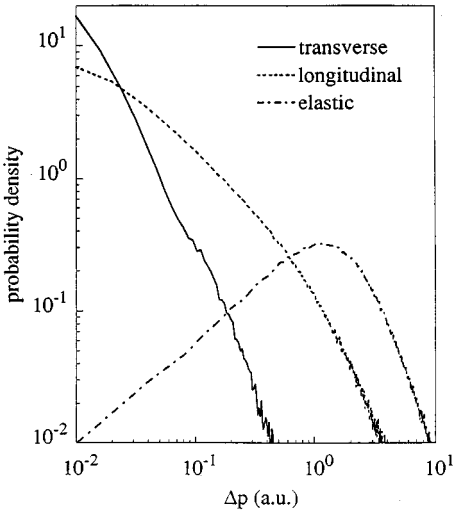

FIG. 7. Momentum transfer distribution $W_\alpha(\Delta p)$ versus the magnitude Δp for inelastic transverse, inelastic longitudinal, and elastic collisions at $v=100$ a.u.

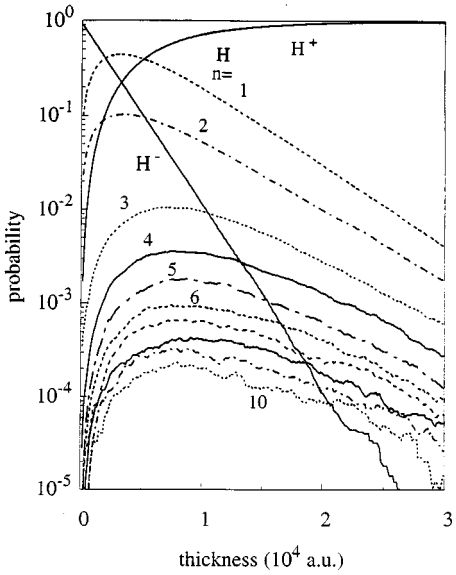

FIG. 8. Population of H^-, H^+, and H(n), $n=1,...,10$ versus the thickness at $E_p=500$ MeV.

sessing the validity of classical dynamics for calculating atomic excitation and ionization. As was shown previously [10], classical dynamics is valid when the scaled momentum transfer $\langle\Delta p\rangle/p_n=\langle\Delta p\rangle n\gtrsim\Delta p_0=0.5$. The momentum transfers due to elastic scattering lie well above the critical momentum transfer. However, the momentum transfer due to transverse excitation as well as the low momentum tail of the longitudinal inelastic excitations lie below this threshold for the lowest n states (e.g., $n=1,2$) while they approach the classical regime in the Rydberg limit $n\gg1$. For example, at $v=100$ a.u. we find that 6% of elastic collisions but 68% of longitudinal and nearly 100% of transverse inelastic collisions with momentum transfers below the critical value for $n=1$, $\Delta p_0=\Delta p\simeq0.5$. This deficiency is partially compensated by the fact that the mean free path for transverse excitation (see Table I and Fig. 5) as well as the partial mean free path for soft longitudinal collisions is large. Their statistical weight in the multiple scattering is therefore reduced. Taking into account the respective weight of the different interactions (see Table I), we obtain a total probability of 43% for a momentum transfer lower than Δp_0 for the ground state and smaller values for excited states. Classical dynamics can therefore be expected to be valid with the possible exception of the excitation functions for low-lying states (e.g., $n=1\rightarrow n=2$). The quantum-mechanical treatment of this problem is currently under investigation [11].

V. EXCITED-STATE FORMATION AND SURVIVAL

The evolution of different charge states and different excited states, H(n), of an incident H^- beam as a function of the thickness of the foil is displayed in Fig. 8. The survival probability of H^- follows an exponential decay law. Fluctuations around the exponential curve are a measure of the statistical uncertainty of the Monte Carlo (MC) ensemble simulation. The fraction of fully stripped H^+ increases monotonically. All excited-state fractions of H(n) display a maximum. One significant feature of the survival probability

TABLE II. Shake probability for producing H(n) during detachment of H^- [using Eq. (10)].

n	1	2	3
P_n (shake)	0.801	0.18	0.002

of the bound states versus the thickness is that the maxima of the $n=1$ and 2 distributions are shifted towards smaller thicknesses relative to that of the higher n states. This indicates that the mechanism of production of high n states is different from that of low n states. The shakeup during the detachment of H^- produces predominantly $n=1$ and 2 states of H (see Table II) while excitation to $n\gtrsim3$ occurs with a probability of $<0.5\%$. The $n=1$ and 2 states are therefore produced in a single step, while higher n states are produced in (at least) two steps, which requires an increased path length, or equivalently, a larger thickness. The population of the ground state serves as a source which feeds the higher n shells inaccessible by shakeup. Accordingly, the position of the maximum of $n=3$ lies at a thickness which is a factor 1.7 larger than that for $n=1$. Similar results hold for higher n shells.

All IMFP's with the exception of the IMFP for transverse excitations scale approximately with velocity as v_p^{-2} (neglecting the slowly varying log term). Since transverse excitations are still relatively unimportant at $\gamma\lesssim2$, this scaling property can be employed to determine universal population curves. In Fig. 9 we give the results for H^-, H ($n=1+2$), and H ($n=3$) for different collision velocities ($v_p=80-115$) as a function of thickness in units of the mean free path λ_0. It is clear that the population distribution depends only on the scaled thickness x/λ_0. The influence of relativistic corrections is illustrated in Fig. 10, in which we compare survival

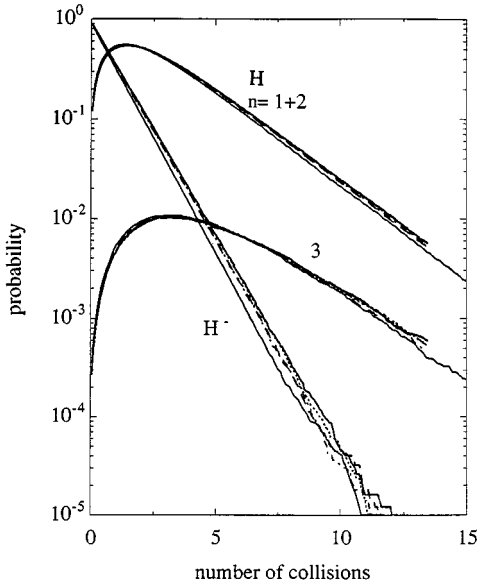

FIG. 9. Fractions of H^-, H ($n=1+2$), and H ($n=3$) versus the scaled thickness x/λ_0, corresponding to the number of collisions, for different energies ($E=800$, 716, 581, 500, and 226 MeV). The statistical error of the MC simulation is comparable to the differences between curves.

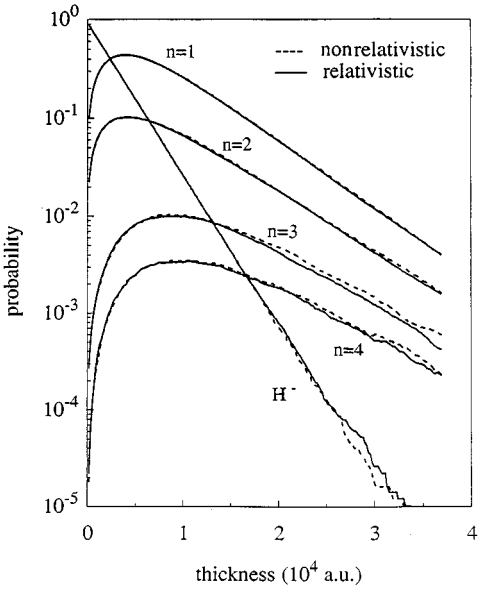

FIG. 10. Comparison between the relativistic and nonrelativistic CTT simulation at $E_p=800$ MeV for H^- and H ($n=1$, 2, 3, and 4) as a function of the thickness.

probabilities for H^- and H(n) ($n=1,\ldots,4$) employing relativistic and nonrelativistic dynamics. Obviously, for moderate values of γ relativistic corrections are not yet important. For larger energies beyond the stopping power minimum, however, the excitation and ionization would be drastically different when the transverse excitations begin to dominate the IMFP.

A comparison between our CTT and recent experimental data of Gulley and co-workers [3] (see accompanying paper) is presented in Fig. 11. Overall, the agreement is remarkably good considering the fact that our simulation represents a fully microscopic theory with no adjustable parameter. The difference between the peak position of populations of the $n=1$ and 2 and of higher n shells clearly indicates that the

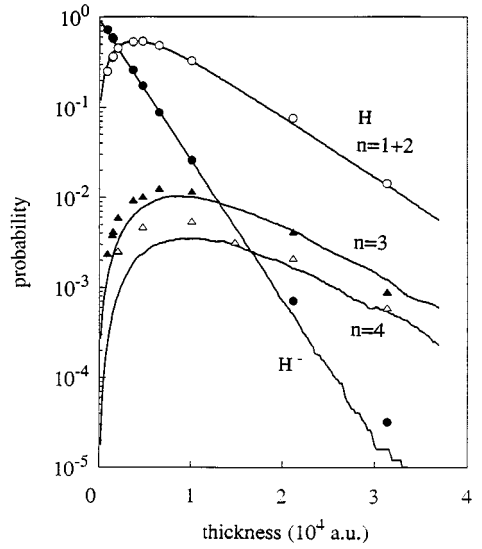

FIG. 11. Comparison of present CTT simulation with absolute experimental data (Ref. [3]) at $E_p=800$ MeV for H^-, H ($n=1+2$), H ($n=3$), and H ($n=4$).

former are formed in a single-step process while the latter require multistep excitation paths. There are, however, a few noticeable deviations, in particular, in the populations at small thicknesses for which, on the average, only one or two collisions have occurred. This suggests the need of improvements of our simulations along two different lines: an improved treatment of the initial shakeup process and a quantum treatment of the excitation of low-lying states since a fraction of characteristic momentum transfers is below the critical threshold where excitation proceeds classically.

VI. RATE EQUATION MODEL

The observation of the universality of the populations as a function of thickness suggests that a simple rate equation model would be capable of describing some of their main features. While less complete than the full simulation, the rate equation model allows the parametrization in terms of a few dominant inverse mean free paths, or equivalently, cross sections which can be compared with the experiment.

For all states, the population is determined by the competition between the production by a source term $S(x)$ per unit length and the probability per unit length to leave the state n, which is proportional to the population of the state n. Thus the population p_n of a given state n at a given thickness x satisfies the following differential equation:

$$\frac{dp_n}{dx}=S-\lambda_n^{-1}p_n, \tag{51}$$

where λ_n^{-1} is the probability per unit length for leaving the state n. The solution p_n is then given by the convolution of the source term with the decay term

$$p_n(x)=\int_0^x S(x')e^{-\lambda_n^{-1}(x-x')}dx'. \tag{52}$$

If we neglect the contribution of the higher n levels to produce the $n=1$ state, the source for the ground state may be represented by an exponential function $S(x)=\alpha_{01}\lambda_0^{-1}p_0(x)$ where $p_0(x)=\exp(-\lambda_0^{-1}x)$ to account for the H^- decay. Here α_{01} is the probability for decay to the $n=1$ state. Equation (52) leads to

$$\begin{aligned}p_1(x)&=\alpha_{01}\lambda_0^{-1}\int_0^x e^{-\lambda_0^{-1}x'}e^{-\lambda_1^{-1}(x-x')}dx'\\&=\frac{\alpha_{01}\lambda_0^{-1}}{\lambda_0^{-1}-\lambda_1^{-1}}\left(e^{-\lambda_1^{-1}x}-e^{-\lambda_0^{-1}x}\right)\end{aligned} \tag{53}$$

in agreement with the result given by Mohagheghi *et al.* [1].

For the $n=2$ state the source term may be approximated by $S(x)=\alpha_{02}\lambda_0^{-1}p_0(x)+\alpha_{12}\lambda_1^{-1}p_1(x)$, if we neglect the contribution from higher n states. α_{02} is the fraction of the population of H^- shaken up into $n=2$ while α_{12} is the fraction of the population of the state $n=1$ excited to $n=2$. The second term in the source function should be smaller than the first since for small thicknesses $p_1(x)\ll p_0(x)$. Furthermore, the IMFP for ionization of H^-, λ_0^{-1}, is larger than the IMFP for destruction of the state $n=1$, λ_1^{-1} because of the smaller binding energy of the detached electron. On the other hand, the branching ratio α_{12}, which should be of the order of the

TABLE III. Inverse mean free paths λ^{-1} and cross sections σ determined by fitting the population curves of the CTT to the rate equations [Eqs. (4), (53), and (56)], $E=800$ MeV. Experimental data from Ref. [3].

Process	λ^{-1} (a.u.)	σ_{theory} (cm^2)	$\sigma_{\text{expt.}}$ (cm^2)
Destruction of H^-	$\lambda_0^{-1}=3.7\times10^{-4}$	6.9×10^{-19}	7.03×10^{-19}
Destruction of H ($n=1$ or 2)	$\lambda_1^{-1}\simeq1.4\times10^{-4}$	2.7×10^{-19}	2.75×10^{-19}
Destruction of H ($n=3$)	$\lambda_3^{-1}\simeq3\times10^{-4}$	5.5×10^{-19}	4.5×10^{-19}
$H^-\rightarrow$H ($n=1$ and 2)		6.4×10^{-19}	6.7×10^{-19}
H ($n=1$ or 2)$\rightarrow$H ($n=3$)		1.8×10^{-20}	1.2×10^{-20}

dipole oscillator strength in the Bethe-Born limit for $1s\rightarrow2p$ excitation $\simeq0.42$ [25], is larger than the branching ratio for shakeup $\alpha_{02}\simeq0.18$. Neglecting the second term in $S(x)$, the population function $p_2(x)$ for $n=2$ coincides with Eq. (53) upon replacing the subscript 1 by 2. The shapes of the $n=1$ and 2 curves therefore closely resemble each other. For both curves the maximum is at

$$x\lambda_0^{-1}=\ln(\tilde{\lambda}^{-1})/(\tilde{\lambda}^{-1}-1), \tag{54}$$

where $\tilde{\lambda}^{-1}=\lambda_{1,2}^{-1}/\lambda_0^{-1}$. Since both λ_1^{-1} and λ_2^{-2} scale approximately as v_p^{-2} with projectile velocity, the position of the maximum in units of the MFP, x/λ_0, is independent of projectile velocity. According to our simulation, for both curves the maximum occurs at the same thickness, implying that $\lambda_1^{-1}\approx\lambda_2^{-1}\approx\lambda_0^{-1}/2$.

For higher-lying states we can assume that the main source term for $n=3$ is provided by the population of the states 1 and 2 instead of H^-. Since $\lambda_1^{-1}\approx\lambda_2^{-1}$ the source term is

$$\begin{aligned}S(x)&=\alpha_{13}\lambda_1^{-1}p_1(x)+\alpha_{23}\lambda_2^{-1}p_2(x)\\&\approx\frac{\lambda_0^{-1}\lambda_1^{-1}}{\lambda_0^{-1}-\lambda_1^{-1}}(\alpha_{02}\alpha_{23}+\alpha_{01}\alpha_{13})(e^{-\lambda_1^{-1}x}-e^{-\lambda_0^{-1}x}).\end{aligned} \tag{55}$$

Consequently, the fraction of atoms in the state $n=3$ (or higher) is

$$\begin{aligned}p_3(x)=\frac{\lambda_0^{-1}\lambda_1^{-1}}{\lambda_0^{-1}-\lambda_1^{-1}}(\alpha_{02}\alpha_{23}+\alpha_{01}\alpha_{13})\Bigg(&\frac{e^{-\lambda_1^{-1}x}-e^{-\lambda_3^{-1}x}}{\lambda_3^{-1}-\lambda_1^{-1}}\\&-\frac{e^{-\lambda_0^{-1}x}-e^{-\lambda_3^{-1}x}}{\lambda_3^{-1}-\lambda_0^{-1}}\Bigg).\end{aligned} \tag{56}$$

The population curve $p_3(x)$ reaches its maximum at larger values of x which serves as a clear signature that this state is formed by a multistep rather than a single-step process. Populations of high n shells can also be described by the same functional form [Eq. (56)], however, with different parameters.

Equations (4), (53), and (56) can be fitted to the numerical results of the CTT (Fig. 11) to extract estimates for the inverse mean free paths λ_0, λ_1, and λ_3 corresponding to destruction cross sections σ_0, σ_1, σ_3 for the initial states H^-, H ($n=1$ or 2), and H ($n=3$). Furthermore, through determination of the branching ratios α_{0i} a few state-selective cross sections for stripping from H^- to H ($n=1$ and 2), $\sigma_{0;1+2}$ and excitation H ($n=1$ or 2) to H ($n=3$), $\sigma_{1,2;3}$ can be estimated. Results and a comparison with the experiment [3] are given in Table III. The overall agreement is satisfactory. As expected, the largest discrepancy appears in the excitation cross section for small n ($n=1$ and 2).

VII. SUMMARY

We have presented a theoretical description of excited-state formation of H and of ionization of H^- ions penetrating solid targets at moderately relativistic speeds with $\gamma\leqslant2$ ($E_p\leqslant1$ GeV). We show that relativistic corrections of the collisional momentum transfer due to the onset of transverse electromagnetic excitations in the medium are not yet important in this energy regime but may become so at higher energies $E_p>1$ GeV. Formation of low-lying states of H proceeds predominantly by a single collision resulting in detachment and shakeup of the second electron. Higher-lying states are predominantly formed in a multiple scattering sequence requiring at least two steps. We find good agreement with recent experimental data for 800-MeV projectiles penetrating thin carbon foils.

The present calculation deals with the populations of n shells. Since stripping by external fields is highly state selective with respect to parabolic substates, future investigations will focus on the calculation of the thickness dependence of the population of individual substates. A reliable determination of substate populations will require a more detailed treatment of the primary shake process. Furthermore, we plan to study the redistributions among low-lying states within the framework of a quantum transport theory.

ACKNOWLEDGMENTS

This work has been supported by the National Science Foundation and by the U. S. Department of Energy, Office of Basic Sciences, Division of Chemical Sciences, under Contract No. DE-AC05-96OR22464 with Lockheed Martin Energy Research Corp. and by a NATO travel grant.

[1] A. H. Mohagheghi, H. C. Bryant, P. G. Harris, R. A. Reeder, H. Sharifian, C. Y. Tang, H. Tootoonchi, C. R. Quick, S. Cohen, W. W. Smith, and J. E. Stewart, Phys. Rev. A **43**, 1345 (1991).

[2] J. Burgdörfer and J. Gibbons, Phys. Rev. A **42**, 1206 (1990); J. Burgdörfer, in *The Physics of Electronic and Atomic Collisions* (XVI International Conference), edited by A. Dalgarno, R. Freund, P. Koch, M. Lubell, and T. Lucatorto, AIP Conf. Proc. No. 205 (AIP, New York, 1990), p. 476.

[3] M. S. Gulley, P. B. Keating, H. C. Bryant, E. P. Mackerrow, W. A. Miller, D. C. Rislove, S. Cohen, J. B. Donahue, D. H. Fitzgerald, S. C. Frankle, D. J. Funk, R. L. Hutson, R. J. Macek, M. A. Plum, N. G. Stanciu, O. B. van Dyck, C. A. Wilkinson, and C. W. Planner (unpublished).

[4] B. Gervais and J. Burgdörfer, Nucl. Instrum. Methods Phys. Res. Sect. B **99**, 101 (1995).

[5] A. Dalgarno and H. Sadeghpour, Phys. Rev. A **46**, R3591 (1992); A. Dalgarno and R. W. Stewart, Proc. Phys. Soc. London **80**, 616 (1962).

[6] L. H. Andersson, P. Hvelplund, S. P. Møller, A. H. Sorensen, K. Elsener, K. G. Rensfedt, and E. Uggerhoj, Phys. Rev. A **36**, 3612 (1987); A. Müller, W. Groh, U. Kneissl, R. Heil, H. Ströher, and E. Salzborn, J. Phys. B **16**, 2039 (1983).

[7] A. L. Ford and J. Reading, J. Phys. B **21**, L685 (1988); J. Wang, J. McGuire, and J. Burgdörfer, Phys. Rev. A (to be published).

[8] J. Levin, I. Sellin, B. Johnson, D. Lindle, R. Miller, N. Berrah, Y. Azuma, H. G. Berrah, and D. H. Lee, Phys. Rev. A **47**, R16 (1993).

[9] F. Byron and C. Joachain, Phys. Rev. **164**, 1 (1967); T. Åberg, Phys. Rev. A **2**, 1726 (1970); L. R. Andersson and J. Burgdörfer, Phys. Rev. Lett. **71**, 50 (1993).

[10] C. O. Reinhold and J. Burgdörfer, J. Phys. B **26**, 3101 (1993); J. Burgdörfer and C. O. Reinhold, *Symposium on Two-Center Effects in Ion-Atom Collisions in honor of M. Rudd*, AIP Conf. Proc. (AIP, New York, in press).

[11] T. Åberg, Ann. Acad. Sci. Fen. AVI **306**, 1 (1969); L. Andersson and J. Burgdörfer, Phys. Rev. A **50**, R2810 (1994).

[12] J. Wang, J. H. McGuire, and J. Burgdörfer, Phys. Rev. A **51**, 4687 (1995).

[13] S. Chandrasekhar, Astrophys. J. **100**, 176 (1944).

[14] L. H. Thomas, Proc. R. Soc. London, Ser. A **114**, 561 (1927).

[15] R. Shakeshaft and L. Spruch, Rev. Mod. Phys. **51**, 369 (1979); J. Briggs and K. Dettmann, Phys. Rev. Lett. **33**, 1123 (1974).

[16] R. Abrines and I. C. Percival, Proc. Phys. Soc. London **88**, 861 (1966); R. Becker and A. MacKellar, J. Phys. B **17**, 3923 (1984).

[17] H. S. Snyder and W. Scott, Phys. Rev. **76**, 220 (1949); N. F. Mott and H. S. W. Massey, *The Theory of Atomic Collision* (Oxford University Press, New York, 1965).

[18] J. Neufeld and R. H. Ritchie, Phys. Rev. **98**, 1632 (1955); **99**, 1125 (1955).

[19] U. Fano, Phys. Rev. **102**, 385 (1956); **103**, 1202 (1956); Annu. Rev. Nucl. Sci. **13**, 1 (1963).

[20] J. C. Ashley, J. J. Cowan, R. H. Ritchie, V. E. Anderson, and J. Hoelzl, Thin Solid Films **60**, 361 (1979).

[21] V. A. Fomichev and I. I. Zhukova, [Opt. Spectrosc. (USSR) **24**, 147 (1968)].

[22] E. T. Arakawa, S. M. Dolfini, J. C. Ashley, and M. W. Williams, Phys. Rev. B **31**, 2655 (1992).

[23] C. O. Reinhold, J. Burgdörfer, J. Kemmler, and P. Koschar, Phys. Rev. A **45**, 2655 (1992).

[24] E. A. Taft and H. R. Philipp, Phys. Rev. **135**, A197 (1965).

[25] H. Bethe and E. Salpeter, *Quantum Mechanics of One- and Two-Electron Atoms* (Plenum Press, New York, 1977).